# Evidence for a Bis(Elongated $\sigma$)-Dihydrideborate Coordinated to Osmiun

*Juan C. Babón,*[a] *Miguel A. Esteruelas,**[a] *Israel Fernández,*[b] *Ana M. López,*[a] *and Enrique Oñate*[a]

[a]Departamento de Química Inorgánica, Instituto de Síntesis Química y Catálisis Homogénea (ISQCH), Centro de Innovación en Química Avanzada (ORFEO-CINQA), Universidad de Zaragoza-CSIC, 50009 Zaragoza, Spain

[b]Departamento de Química Orgánica I, Facultad de Ciencias Químicas, Centro de Innovación en Química Avanzada (ORFEO-CINQA), Universidad Complutense de Madrid, 28040 Madrid, Spain

**ABSTRACT** The formation and Atoms in Molecules (AIM) analysis of osmium(IV) and osmium(II) complexes containing dihydrideborate groups and primary aminoborane ligands are reported. Complex $OsH_6(P^iPr_3)_2$ (**1**) loses a hydrogen molecule and the resulting unsaturated $OsH_4(P^iPr_3)_2$ species coordinates 9-borabicycle[3.3.1]nonane (HBbn) and pinacolborane (HBpin) to give the dihydrideborate derivatives $OsH_3\{\kappa^2\text{-}H,H\text{-}(H_2BR_2)\}(P^iPr_3)_2$ ($BR_2$ = Bbn (**2**), Bpin (**3**)). The bonding situation in these compounds and in the related osmium(II) derivative $Os(Bcat)\{\kappa^2\text{-}H,H\text{-}(H_2Bcat)\}(CO)(P^iPr_3)_2$ (**4**) (HBcat = catecholborane) has been analyzed by the AIM method. The Laplacian distributions in the Os–H–B plane exhibit a four-membered cyclic topology

possessing two Os–H and two B–H bond critical points associated with one OsHHB ring critical point, which resembles that found for $B_2H_6$. The tetrahydride $OsH_4(P^iPr_3)_2$ also coordinates catecholborane, which initially affords $OsH_3\{\kappa^2\text{-}H,H\text{-}(H_2Bcat)\}(P^iPr_3)_2$ (**5**). In contrast to **2** and **3**, complex **5** reacts with a second molecule of HBcat to give the elongated $\sigma$-borane-{bis(elongated $\sigma$)-dihydrideborate}-osmium(II) derivative $OsH(\eta^3\text{-}H_2Bcat)(\eta^2\text{-}HBcat)(P^iPr_3)_2$ (**6**). Complexes **5** and **6** have been also analyzed by the AIM method. Complex **5** displays the same topology as **2**–**4**. However, the $OsH_2B$ unit of **6** shows, besides the Os–H and B–H bond critical points, an additional Os–B bond critical point, which is associated with a bond path running between these atoms. This double triangular topology is completed with the respective ring critical points. Reactions of **1** with dimethylamine–borane ($H_3B{\cdot}NHMe_2$) and *tert*-butylamine–borane ($H_3B{\cdot}NH_2{}^t$Bu) give $OsH_2(\eta^2\text{:}\eta^2\text{-}H_2BNR_2)(P^iPr_3)_2$ ($NR_2$ = $NMe_2$ (**7**), $NH^t$Bu (**8**)). The AIM analyses of **7** and **8** also reveal the occurrence of an Os–B bond critical point associated with a bond path running between those atoms. However, neither Os–H bond critical points nor bond paths are observed in the latter species.

## INTRODUCTION

The first step in the homolytic and heterolytic cleavage of $\sigma$-bonds promoted by transition metal complexes is the coordination of the $\sigma$-bond to an unsaturated metal fragment, to form a $\sigma$-complex.[1] The electronic nature of the latter determines the homolysis or heterolysis of the coordinated bond. Molecular hydrogen is the best known case, with four well established situations, namely Kubas-type dihydrogen, elongated dihydrogen, compressed dihydrides, and classical dihydrides.[1,2]

The study of the coordination of B–H bonds to transition metal complexes is much more difficult than the investigation of the metal-dihydrogen interaction.[3] However, the effort is worth it due to the connection of the B–H bond activation reactions with the borylation of organic molecules[4] and the dehydrocoupling of amine–boranes.[5] In this context, the Atoms in Molecules (AIM) method is really helpful,[6] although it has been scarcely applied to these particular systems. According to the AIM method, the $\sigma$(B–H)-complexes can be classified into the following groups: bis($\sigma$)-borane (**I**),[7] $\sigma$, elongated $\sigma$-borane (**II**),[7b] bis(elongated $\sigma$)-borane (**III**),[8] $\sigma$-borinium (**IV**),[1,9] $\sigma$-borane (**V**),[10] and elongated $\sigma$-borane (**VI**)[10,11] (Chart 1). The analysis of the electron density involved in the M($\eta^2$-H–B) bonds reveals two main topologies. While the coordinated elongated $\sigma$-BH bonds give rise to a triangular topology involving M–B, M–H, and B–H bond critical points (BCPs) and a ring critical point (RCP),[12] the coordinated $\sigma$-BH bonds only display M–B and B–H bond critical points; i.e., they lack a similar triangular topology. Figure 1 illustrates that for the BH-borane coordination.[10]

**Chart 1. Types of σ(B–H)-complexes**

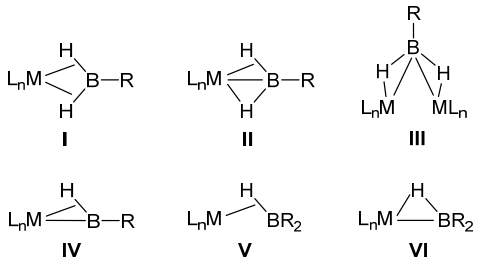


(a) Elongated σ-Borane (b) σ-Borane

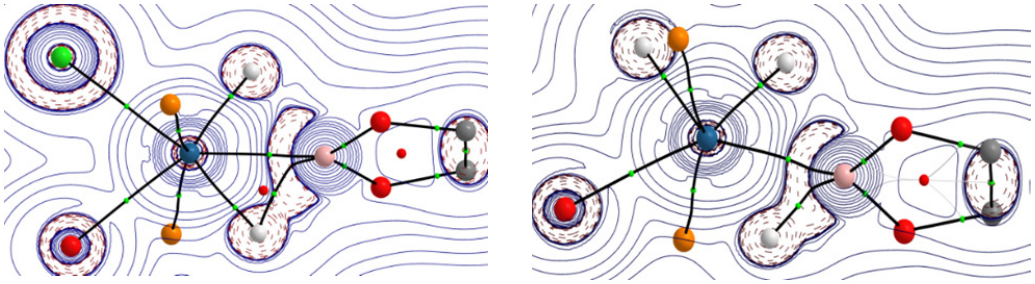

**Figure 1**. Contour line diagrams $\nabla^2\rho(r)$ for the elongated σ-borane OsHCl($\eta^2$-HBcat){$\kappa^3$-*P*,*O*,*P*-[xant($P^iPr_2$)$_2$]} (xant($P^iPr_2$)$_2$ = 9,9-dimethyl-4,5-bis(diisopropylphosphine)xanthene) (a) and σ-borane $OsH_2$($\eta^2$-HBcat){$\kappa^3$-*P*,*O*,*P*-[xant($P^iPr_2$)$_2$]} (b) complexes in the O–Os–B plane. The solid lines connecting the atomic nuclei are the bond paths while the small green and red spheres indicate the corresponding BCPs and RCPs, respectively. H (white); B (pink); C (grey); O (red); Cl (green); Os (blue).

Polyhydrides of platinum group metals promote the activation of a wide range of *σ*-bonds, including B–H.[1] The coordination of the latter to an unsaturated compound of this class generates species having up to five different natures: borinium,[9] *σ*-borane,[10,13] elongated *σ*-borane,[10] bis(*σ*)-borane,[14] and dihydrideborate.[15] As the heterolytic activation can be rationalized in terms of the abstraction of the electrophilic fragment of the coordinated bond by a base bonded to the metal center, the metal–dihydrideborate unit can be at first glance viewed as an intermediate situation in the pathway of the hydride-mediated heterolytic rupture of a coordinated B–H bond; i.e., an intermediate situation for the H/H exchange between the metal center and the boron atom in hydride-(σ-borane) complexes. Dihydrideborate is typically characterized by the AIM method as a four-membered cycle possessing two M–H and two B–H bond critical points associated with one MHHB ring critical point.[16] This particular topology, where the bond paths are inwardly curved, strongly resembles the situation found in $B_2H_6$ (Figure 2).[17]

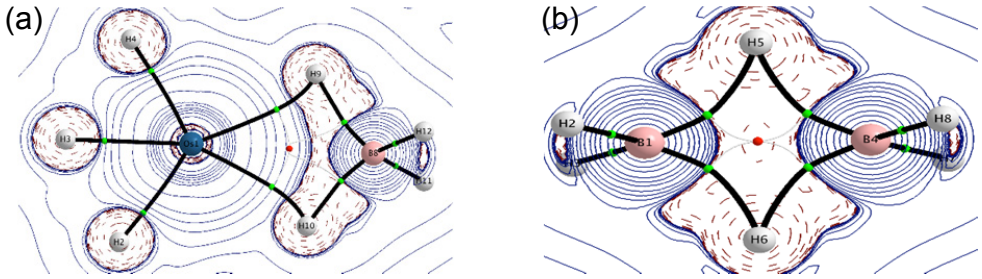


**Figure 2**. Contour line diagrams $\nabla^2\rho(r)$ for complex $OsH_3(\kappa^2\text{-}H_2BH_2)(IPr)(PPh_3)$ (IPr = 1,3-bis(2,6-disopropylphenyl)-Imidazolylidene) in the Os–H–B plane (a) and $B_2H_6$ in the plane of the bridging hydrogen atoms (b). The solid lines connecting the atomic nuclei are the bond paths while the small green and red spheres indicate the corresponding BCPs and RCPs, respectively. H (white); B (pink); C (grey); Os (blue).

Osmium probably exhibits the richest polyhydride chemistry among the platinum group metals.[1] However, the activation of B–H bonds by osmium-polyhydride complexes has received very little attention,[18] in particular when compared to ruthenium.[3b] The $d^2$-hexahydride $OsH_6(P^iPr_3)_2$ (**1**) promotes the heterolytic cleavage of C–H,[19] N–H,[20] and O–H[21] bonds, in addition to the activation of C–C, C–N,[22] and C–O[23] bonds. As a consequence of its saturated nature, the first step of these processes involves the release of a hydrogen molecule from the osmium coordination sphere to afford the unsaturated $d^4$-tetrahydride $OsH_4(P^iPr_3)_2$, which has been trapped with pyridines (Scheme 1).[24] Our interest in the B–H bond activation reactions,[9a,10,13b,15h,18] prompted us to investigate the addition of 9-borabicycle[3.3.1]nonane dimer ($(HBbn)_2$), pinacolborane (HBpin), catecholborane (HBcat), and amine–boranes to this tetrahydride. The study has allowed us to obtain experimental and AIM evidence for an unprecedented dihydrideborate coordination mode, bis(elongated $\sigma$)-dihydrideborate, in addition to prepare novel dihydrideborate and bis($\sigma$)-aminoborane complexes in the osmium chemistry.

**Scheme 1. Reactions of 1 with Pyridine and Substituted Pyridines**

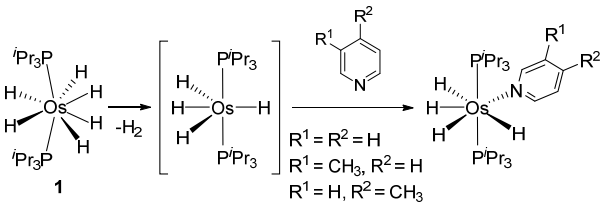


We herein report the preparation, complete characterization, and AIM analyses of trihydride-dihydrideborate-osmium(IV) complexes, hydride-(elongated σ-borane)-{bis(elongated σ)-dihydrideborate}-osmium(II) species, and dihydride-{bis(σ)-aminoborane}-osmium(II) derivatives (Scheme 2).

**Scheme 2. Reactions of 1 with Boranes and Amine-Boranes**

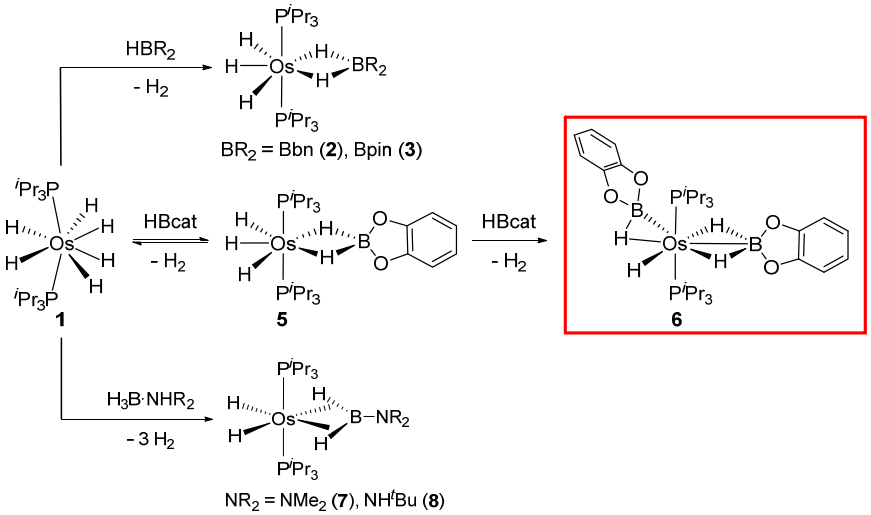


## RESULTS AND DISCUSSION

**Trihydride-Dihydrideborate-Osmium(IV) Complexes.** The heating of toluene solutions of the hexahydride complex **1**, at 110º C, in the presence of 0.5 mol of $(HBbn)_2$, for 18 h gives rise to the quantitative formation of $OsH_3\{\kappa^2\text{-}H,H\text{-}(H_2Bbn)\}(P^iPr_3)_2$ (**2**), as a result of the addition of the B–H bond of the monomer HBbn to an Os–H bond of the tetrahydride $OsH_4(P^iPr_3)_2$. Similarly, the heating of toluene solutions of **1**, at 50 ºC, in the presence of 2 mol of HBpin, for

18 h affords the Bpin-counterpart $OsH_3\{\kappa^2\text{-}H,H\text{-}(H_2Bpin)\}(P^iPr_3)_2$ (**3**). These compounds were isolated as yellow (**2**) and white (**3**) solids, according to Scheme 2, in moderated yield (50-30%) due to their high solubility in usual organic solvents. Notably, although some tetrahydrideborate complexes of osmium(II)[25] and osmium(IV)[17,26] have been reported, as far as we know, the boryl-osmium(II) species $Os(Bcat)(CO)\{\kappa^2\text{-}H,H\text{-}(H_2Bcat)\}(P^iPr_3)_2$ (**4**) is the only dihydrideborate derivative of this element which has been previously characterized.[15h]

Figure 3a shows a view of the X-ray diffraction analysis structure of **2** which proves the formation of the dihydrideborate ligand and its $\kappa^2$-*H*,*H*-coordination. The geometry around the osmium atom can be rationalized as a distorted pentagonal bipyramid with the phosphines occupying axial positions (P–Os–P = 167.33(2)°). The metal coordination sphere is completed with the dihydrideborate group and the hydride ligands. The former acts with a H(01)–Os–H(02) bite angle of 65.0(13)°. The separation between the metal center and the borate boron atom of 2.355(3) Å is consistent with other crystallographically characterized osmium-tetrahydrideborate complexes.[15h,17,26a] According to a $sp^3$-hybridation, the angles around the boron atom are between 113.6(7)° and 98.9(19)°. The bonds between the metal center and the boron bridging hydrogen atoms appear to be weaker than the osmium-hydride bonds. Thus, the Os–H(01) and Os–H(02) bond lengths of 1.79(3) and 1.83(3) Å are about 0.2 Å longer than the osmium hydride distances of 1.578(10) (Os–H(03)), 1.573(10) (Os–H(04)), and 1.581(10) (Os–H(05)) Å. The separations between the central hydride H(04) and those of the corners are 1.45(4) and 1.76(4) Å, respectively. The DFT optimized structure (BP86-D3/def2-TZVPP level) confirms the classical nature of the hydride ligands, which display separations of 1.620 (H(03) and H(04)) and 1.643 (H(04) and H(05)) Å, and the differences in length of the Os–H bonds, which lie about 1.62 Å for the hydrides and about 1.82 Å for the boron bridging hydrogen atoms. Figure 3b shows the

Laplacian distribution for **2** in the Os–H–B plane. In agreement with the dihydrideborate nature of the boron ligand, this compound is characterized by the AIM method as a four-membered cyclic species possessing two Os–H and two B–H bond critical points associated with one OsHHB ring critical point.

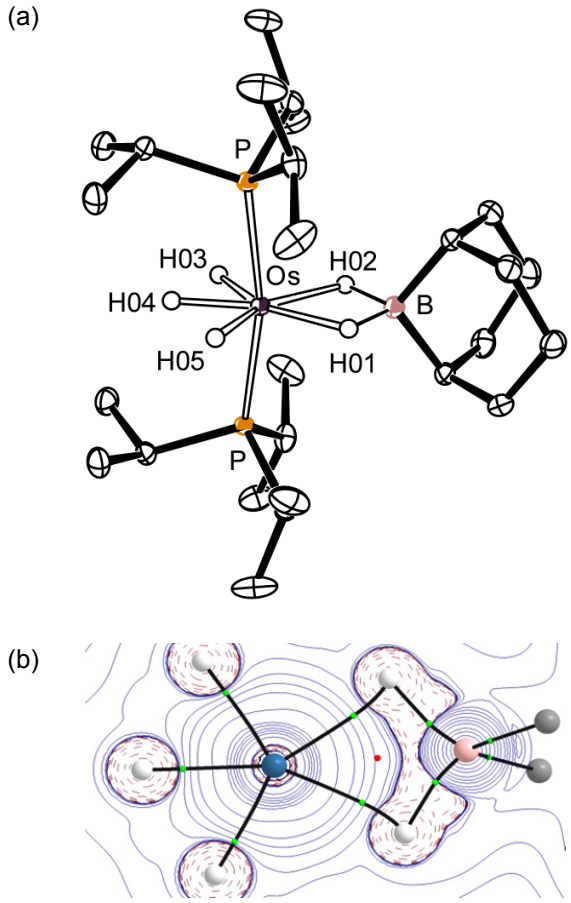


**Figure 3.** (a) Molecular diagram of complex **2** with 50% probability ellipsoids. Hydrogen atoms (except hydrides) are omitted for clarity. Selected bond lengths (Å) and angles (deg) for the X-ray and optimized (in square brackets) structures: Os–H(01) = 1.79(3) [1.823], Os–H(02) = 1.83(3) [1.827], Os–H(03) = 1.578(10) [1.623], Os–H(04) = 1.573(10) [1.624], Os–H(05) = 1.581(10) [1.625], Os–B = 2.355(3) [2.366], Os–P = 2.3438(5) [2.350], B–H(01) = 1.26(3) [1.338], B–H(02) = 1.30(3) [1.332]; P–Os–P = 167.33(2) [167.21], H(01)–Os–H(02) = 65.0(13)

[68.32], H(02)–Os–H(03) = 84.8(14) [83.24], H(03)–Os–H(04) = 54.8(14) [59.85], H(04)–Os–H(05) = 67.8(16) [60.76], H(05)–Os–H(01) = 87.7(14) [87.84], H(01)–B–H(02) = 98.9(19) [100.27], H(01)–B–C(1) = 113.6(7) [111.38], H(02)–B–C(1) = 112.0(7) [113.02], C(1)–B–C(1) = 106.8(2) [107.73]. (b) Contour line diagram $\nabla^2\rho(r)$ for complex **2** in the Os–H–B plane. The solid lines connecting the atomic nuclei are the bond paths while the small green and red spheres indicate the corresponding BCPs and RCPs ring critical points, respectively.

The $^1$H NMR spectrum of **2** in toluene-$d_8$ is temperature dependent. Figure 4 shows the spectrum in the high field region as a function of the temperature. Between 263 and 233 K it contains a broad signal centered at –10.40 ppm, corresponding to five hydrogen atoms bonded to the metal center. However, at temperatures lower than 203 K, two broad resonances at –12.59 and –7.09 ppm due to the inequivalent hydrides and the equivalent boron bridging hydrogen atoms are observed. This behavior is consistent with the existence of two intramolecular position exchange processes which are thermally activated (Scheme 3). The process having a lower energy barrier, which only involves the hydride ligands ($H^C$ and $H^T$), is characteristic for $OsH_3L_2(P^iPr_3)_2$ species and seems to take place via dihydrogen intermediates.[27] The higher energy barrier process corresponds to the position exchange between the hydride ligands and the boron bridging hydrogen atoms ($H^B$). It has an activation energy of 8.6±0.3 kcal·mol$^{-1}$ and very likely occurs via a tetrahydride-$\sigma$-borane intermediate,[15h,17,26c,28] a transitory species for the formation of **2**. The $^{31}$P{$^1$H} NMR spectrum shows a singlet at 43.8 ppm, whereas the $^{11}$B{$^1$H} NMR spectrum contains a broad signal at 44 ppm.

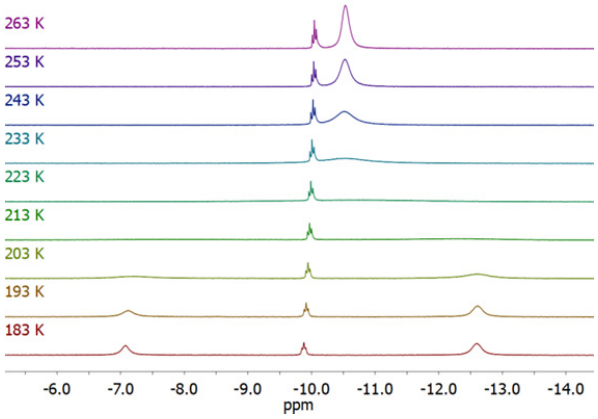


**Figure 4.** High-field region of the $^{1}$H NMR (400.13 MHz, $C_7D_8$) spectrum of complex **2** between 263 and 183 K. The triplet signal at –9.8 belongs to a small amount of $OsH_6(P^iPr_3)_2$.

**Scheme 3. Exchange Processes in 2 and 3**

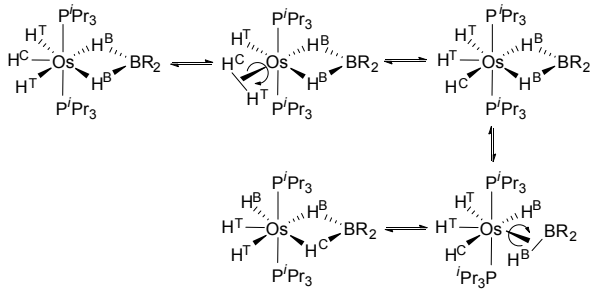

Complex **3** was also characterized by X-ray diffraction analysis. The structure resembles that of **2** with a Bpin group instead of the Bbn unit. Similar to the latter, the AIM method locates two Os–H and two B–H bond critical points associated with a ring critical point in a four-membered cyclic array (Figure S1). The $^{1}$H NMR spectrum of **3**, in toluene-$d_8$, at room temperature contains a high field resonance at −10.30 ppm. In contrast to **2**, it does not decoalesce even at 183 K. This suggests that the interaction between the metal center and the $\sigma$-borane ligand in the seven-coordinate tetrahydride-$\sigma$-borane species, key for the exchange between the hydride ligands and the boron bridging hydrogen atoms, is stronger with HBbn than with HBpin. This agrees with the higher acidity of the boron atom of HBbn with respect to HBpin, which allows a stronger

osmium-to-boron $\pi$-backbonding in the former. A singlet at 44.7 ppm in the $^{31}P\{^{1}H\}$ NMR spectrum and a broad signal at 35 ppm in the $^{11}B\{^{1}H\}$ NMR spectrum are also characteristic features of **3**.

**Hydride-(Elongated σ-Borane)-{bis(Elongated σ)-Dihydrideborate}-Osmium(II) Species.** The hexahydride complex **1** also reacts with HBcat (Scheme 2). The reaction initially affords the Bcat-counterpart of **2** and **3**, $OsH_3\{\kappa^2\text{-}H,H\text{-}(H_2Bcat)\}(P^iPr_3)_2$ (**5**). However, in this case, a second molecule of HBcat displaces a hydrogen molecule of **5** to give $OsH(\eta^3\text{-}H_2Bcat)(\eta^2\text{-}HBcat)(P^iPr_3)_2$ (**6**) before the first reaction is completed. Thus, the addition of 1 mol of HBcat to toluene solutions of **1** leads to a 15:77:8 mixture of **1**, **5**, **6**, after 18h, at 50 °C. Under the same conditions, the treatment of **1** with 3 mol of HBcat gives rise to the quantitative formation of **6**, although it was isolated as colorless crystals in only 27 % yield due to its high solubility in usual organic solvents.

The DFT optimized structure and AIM diagram of **5** (Figure S2) reveal that there are no significant differences either between its dihydrideborate ligand and those of **2** and **3** or in its coordination to the metal center. Thus, the separation between the osmium and boron atoms, 2.286 Å, and the distance between the metal center and the boron hydrogen atoms, 1.783 Å, are very similar to those of **2** and **3**. The $^{1}H$, $^{31}P\{^{1}H\}$, and $^{11}B\{^{1}H\}$ NMR spectra of **5** in toluene-$d_8$ are also in agreement with those of **3**. The $^{1}H$ NMR spectrum between 298 and 183 K contains a broad resonance at –9.61 ppm for the five hydrogen atoms attached to the metal center. In the $^{31}P\{^{1}H\}$ NMR spectrum, the equivalent phosphines display a singlet at 48.0 ppm, whereas the $^{11}B\{^{1}H\}$ NMR spectrum shows a broad signal centered at 40 ppm.

Complex **6** was characterized by X-ray diffraction analysis. The structure (Figure 5a) proves the $\eta^2$-coordination of the B–H bond of the borane and the $\eta^3$-coordination of the $H_2B$ unit of the

dihydrideborate. Like an $\eta^3$-allyl ligand, the latter occupies two coordination positions and donates 3e to the metal center. Thus, the coordination polyhedron around the osmium atom can be rationalized as a distorted octahedron with *trans* phosphines (P(1)–Os–P(2) = 157.22(3)°). The perpendicular plane is formed by the dihydrideborate group, the hydride ligand and the B–H bond of HBcat with the hydrogen atom pointing towards the hydride. The borane B–H bond undergoes elongation as a consequence of its coordination. The B(1)–H(1) bond length of 1.39(3) Å, 1.445 Å in the DFT-optimized structure, is about 0.3 Å longer than in the free borane (1.100 Å)[29] but between 0.1 and 0.3 Å shorter than the B–H distances reported for the elongated $\sigma$-borane derivatives OsHCl($\eta^2$-HBR$_2$){$\kappa^3$-*P*,*O*,*P*-[xant(P$^i$Pr$_2$)$_2$]} (BR$_2$ = Bcat (1.60-1.68 Å), Bpin (1.62-1.69 Å))[10] and Rh($\eta^5$-C$_5$Me$_5$)(Bpin)$_2$($\eta^2$-HBpin) (1.53(2) and 1.69(3) Å).[30] However, it is similar to that found in the iridium complex Ir{$\kappa^3$-*P*,*C*,*P*-[C$_6$H$_3$-1,3-OP$^t$Bu$_2$]}($\eta^2$-HBpin) (1.47(6) Å).[13a] The B(1)–Os–H(1) angle of 41.0(11)°, 42.81° in the optimized structure, is smaller than the related B–M–H bond in the above mentioned compounds (45–55°). This suggests that in this case there is a remarkably strong interaction between the coordinated $\sigma$-bond and the metal center. Indeed the Os–B(1) bond length of 2.112(4) Å compares well with the reported osmium boryl distances.[15h,18a,b,31] The most noticeable feature of the coordination of the dihydrideborate group is the Os–B(2) distance of 2.159(4) Å, which is similar to the Os–B(1) bond length and between 0.1 and 0.2 Å shorter than the separation between the metal center and the boron atom of the dihydrideborate group in **2** and **3**. This shortening is a strong evidence in favor of a significant osmium-boron bonding interaction in the coordinated dihydrideborate. According to the DFT-optimized structure, the Os–H$^B$ distances are 1.793 (Os–H(2)) and 1.730 (Os–H(3)) Å; i.e., they are rather similar despite the hydrogen atoms lie *trans* to different ligands, and also similar to those in **2**, **3**, and **5**. Interestingly, in contrast to the Os–H$^B$ distances, the B–H bond

lengths are sensitive to the ligand *trans* disposed. Thus, the B(2)–H(3) distance (*trans* to B(1)–H(1)) of 1.58(3) Å, 1.440 Å in the calculated structure, is between 0.18 and 0.08 Å longer than the B(2)–H(2) bond length (*trans* to H(01)) of 1.40(3) Å, 1.363 Å in the optimized structure.

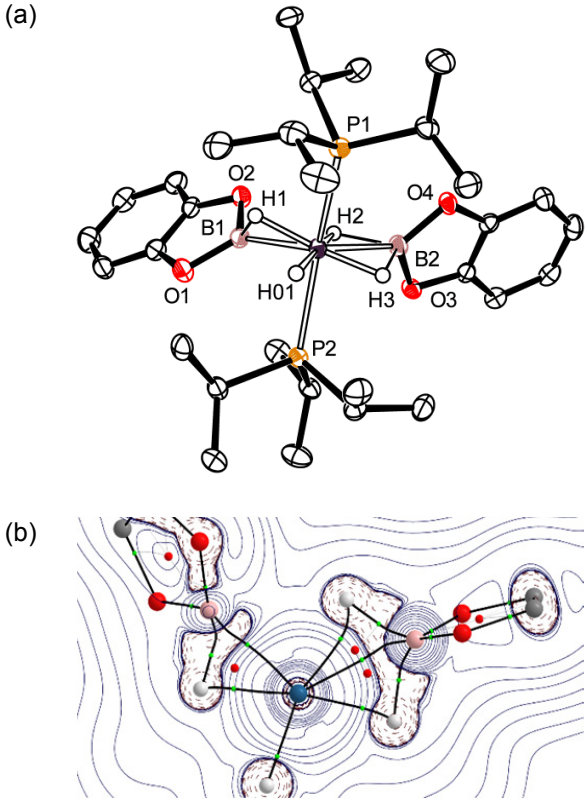


**Figure 5**. (a) Molecular diagram of complex **6** with 50% probability ellipsoids. Hydrogen atoms (except hydrides) are omitted for clarity. Selected bond lengths (Å) and angles (deg) for the X-ray and optimized (in square brackets) structures: Os–H(1) = 1.692(10) [1.701], Os–H(01) = 1.69(3) [1.649], Os–H(2) = 1.692(10) [1.793], Os–H(3) = 1.690(10) [1.730], Os–B(1) = 2.112(4) [2.114], Os–B(2) = 2.159(4) [2.215], Os–P(1) = 2.3518(8) [2.384], Os–P(2) = 2.3805(8) [2.365], B(1)–H(1) = 1.39(3) [1.445], B(2)–H(2) = 1.40(3) [1.363], B(2)–H(3) = 1.58(3) [1.440]; P(1)–Os–P(2) = 157.22(3) [164.15], B(1)–Os–H(1) = 41.0(11) [42.81], H(01)–Os–H(2) =

178.6(16) [171.11], H(1)–Os–H(3) = 171.3(16) [166.41], H(2)–Os–H(3) = 86.7(16) [78.41], H(01)–Os–H(3) = 92.7(15) [93.41], H(1)–B(1)–O(1) = 109.3(12) [108.29], H(1)–B(1)–O(2) = 117.7(14), [121.29], O(1)–B(1)–O(2) = 107.3(3) [107.56], H(2)–B(2)–H(3) = 102.1(6) [105.17], H(2)–B(2)–O(3) = 105.0(12) [111.32], H(2)–B(2)–O(4) = 122.2(13) [115.11], H(3)–B(2)–O(3) = 112.2(11), [108.99], H(3)–B(2)–O(4) = 107.1(11), [108.87], O(3)–B(2)–O(4) = 108.2(3) [107.26]. (b) Contour line diagram $\nabla^2\rho(r)$ for complex **6** in the Os–H–B plane. The solid lines connecting the atomic nuclei are the bond paths while the small green and red spheres indicate the corresponding BCPs and RCPs ring critical points, respectively.

The analysis of the structural parameters related to the coordination of the dihydrideborate group and their comparison with those related to the borane B–H bond coordination indicate that the dihydrideborate group can be viewed as a ligand bonded to the metal through both $\sigma$-B–H bonds; i.e., as a bis(elongated $\sigma$)-dihydrideborate ligand. The computed AIM diagram strongly supports this formulation (Figure 5b). Indeed, in addition to the Os–H and B–H bond critical points, characteristic of the dihydrideborate ligands, the Laplacian distribution in the Os–H–B plane also exhibits an Os–B bond critical point, which is associated with a bond path running between these atoms. As a consequence, the ring critical point, present in the previously mentioned dihydrideborates, is now converted into two different ring critical points, resulting in two triangular arrangements, typical for elongated $\sigma$-borane derivatives, fused by the Os–B bond path. Because, at first glance, one could think that the unusual coordination of the dihydrideborate of **6** is a consequence of the asymmetry of the complex in the Os–H–B plane and/or the different oxidation state of the metal center, +2 in **6** and +4 in **2**, **3**, and **5**, we also analyzed the coordination of the dihydrideborate group of **4** by means of the AIM method. Although complex **4** is also asymmetrical in the Os–H–B plane and its metal center displays a +2

oxidation state, the Laplacian distribution is that expected for a typical dihydrideborate (Figure 6). Therefore, the coordination of the dihydrideborate group in **6** does not depend on either the asymmetry of the complex in the Os–H–B plane or of the oxidation state of the metal center. The calculated Os–B Wiberg Bond Indices (WBI) are consistent with the AIM diagrams. Whereas rather similar WBI values were computed for complexes **2–5** (WBI = 0.36–0.40), a higher WBI of 0.46 was found for **6**.

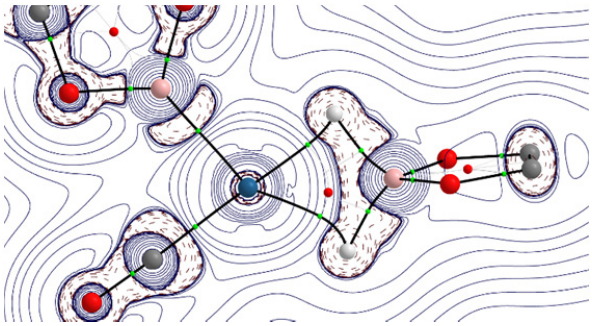

**Figure 6.** Contour line diagram $\nabla^2\rho(r)$ for complex **4** in the Os–H–B plane. The solid lines connecting the atomic nuclei are the bond paths while the small green and red spheres indicate the corresponding BCPs and RCPs ring critical points, respectively.

The Energy Decomposition Analysis (EDA) method was applied next in order to confirm the stronger interaction osmium-dihydrideborate in **6**. To this end, the interactions of the fragments $Os(Bcat)(CO)(P^iPr_3)_2]^+$, $[OsH_3(P^iPr_3)_2]^+$, and $[OsH(\eta^2\text{-}HBcat)(P^iPr_3)_2]^+$ with $[H_2Bcat]^-$ were considered to form complexes **4**, **5**, and **6**, respectively (Table 1). When comparing the osmium(II) species **4** and **6**, it is confirmed that complex **6** benefits from a stronger osmium-dihydrideborate interaction as the computed $\Delta E_{int}$ term is 11.3 kcal·mol$^{-1}$ higher in this compound than in **4**. Closer inspection of the different energy contributions to $\Delta E_{int}$ suggests that this is due to both more stabilizing electrostatic ($\Delta\Delta E_{elstat}$ = 31.8 kcal·mol$^{-1}$) and orbital ($\Delta\Delta E_{orb}$ = 23.7 kcal·mol$^{-1}$) attractions, at expense of the less destabilizing Pauli repulsion computed for **4**

($\Delta\Delta E_{Pauli}$ = 44.2 kcal·mol$^{-1}$). A slightly lower interaction is also computed for the osmium(IV) complex **5**, which also derives from comparatively weaker electrostatic and orbital attractions ($\Delta\Delta E_{elstat}$ = 36.0 kcal·mol$^{-1}$ and $\Delta\Delta E_{orb}$ = 17.4 kcal·mol$^{-1}$).

**Tabla 1. EDA results (in kcal·mol$^{-1}$) computed at the ZORA-BP86-D3/TZ2P//BP86-D3/def2-TZVPP level.**

| | **4** | **5** | **6** |
|---|---|---|---|
| $\Delta E_{int}$ | –163.8 | –173.1 | –175.1 |
| $\Delta E_{Pauli}$ | 197.5 | 188.8 | 241.7 |
| $\Delta E_{elstat}$[a] | –229.0 (63.4%) | –224.8 (62.1%) | –260.8 (62.6%) |
| $\Delta E_{orb}$[a] | –117.3 (32.5%) | –123.6 (34.2%) | –141.0 (33.8%) |
| $\Delta E_{disp}$[a] | –15.0 (4.1%) | –13.5 (3.7%) | –14.9 (3.6%) |

[a] The values within parentheses indicate the percentage to the total attractive interactions energy, $\Delta E_{int} = \Delta E_{Pauli} + \Delta E_{elstat} + \Delta E_{orb} + \Delta E_{disp}$.

The $^{1}$H and $^{11}$B{$^{1}$H } NMR spectra of **6** are unfortunately poorly informative. In the $^{1}$H NMR spectrum, the most noticeable signal is a broad resonance centered –9.5 ppm, which is due to the four inequivalent hydrogen atoms attached to the metal center. Although it broadens upon lowering the sample temperature, decoalescence is not observed even at 148 K in methylcyclohexane-$d_{14}$. A similar behavior is observed in the $^{11}$B{$^{1}$H} spectrum, which contains a broad resonance at 35 ppm, between 298 and 143 K, for the inequivalent boron atoms. The $^{31}$P{$^{1}$H} NMR spectrum shows a singlet at 36.9 ppm for the equivalent phosphines.

**Dihydride-{bis(*σ*)-Aminoborane}-Osmium(II) Derivatives.** Tetrahydride $OsH_4(P^iPr_3)_2$ promotes the release of 1 mol of molecular hydrogen from amine–boranes and captures the resulting aminoborane. The coordination produces the release of a second hydrogen molecule, now from the metal coordination sphere, and the formation of dihydride-{bis(*σ*)-aminoborane}-

osmium(II) derivatives (Scheme 2). Thus, the treatment of toluene solutions of **1** with an excess ($\approx$ 3 mol) of dimethylamine–borane and *tert*-butylamine–borane, at 80 °C, for 18 h leads to $OsH_2(\eta^2{:}\eta^2\text{-}H_2BNR_2)(P^iPr_3)_2$ ($NR_2$ = $NMe_2$ (**7**), $NH^tBu$ (**8**)) and three hydrogen molecules. Complexes **7** and **8** were isolated as colorless crystals in 67% and 20% yield, respectively.

Complex **7** was also characterized by X-ray diffraction analysis. Figure 7a shows a view of the structure. The coordination around the osmium center can be rationalized as a distorted octahedron with mutually *trans* phosphines (P–Os–P = 163.20(2)°). The hydride ligands and the aminoborane group lie at the perpendicular plane. The coordination of the aminoborane resembles that of the alkylborane in the mixed complex $OsH_2(\eta^2{:}\eta^2\text{-}H_2BCH_2Ph)(IPr)(P^iPr_3)$ which, in contrast to **7** and **8**, was prepared by reduction of the Os–C triple bond of the alkylidyne $OsH(OH)(\equiv CPh)(IPr)(P^iPr_3)$ with $Na[BH_4]$.[7c] The separation between the metal center and the boron atom of 1.943(3) Å is statistically identical to that found in the alkylborane (1.913(4) Å) and about 0.2 Å shorter than the Os–B(2) distance in **6**. In this context, it should be noted that the boron atom formally contributes with 2e to the $OsH_2B$ bond in **7** and with 1e in **6**. In contrast to the Os–B distance, the Os–$H^B$ bond lengths of 1.807 (Os–H(03)) and 1.839 (Os–H(04)) Å are about 0.1 Å longer, according to the DFT-optimized structures. Nevertheless, the B–H distances of 1.382 (B–H(03)) and 1.362 (B–H(04)) Å are similar to the length of the bond B(2)–H(2) in **6**, which is also disposed *trans* to a hydride ligand. The AIM diagram of **7** (Figure 7b) is the expected one for a bis($\sigma$)-borane derivative[7] and fully consistent with its X-ray diffraction analysis structure. Therefore, it shows significant differences with that of **6**. Like in the latter, the Laplacian of the electron density in the Os–H–B plane exhibits a significant Os–B interaction as revealed by the occurrence of a bond critical point located between the transition metal and the boron atom, which is associated with a bond path running between both atoms.

However, in contrast to **6**, no Os–$H^B$ bond critical points or bond paths nor ring critical points are observed.

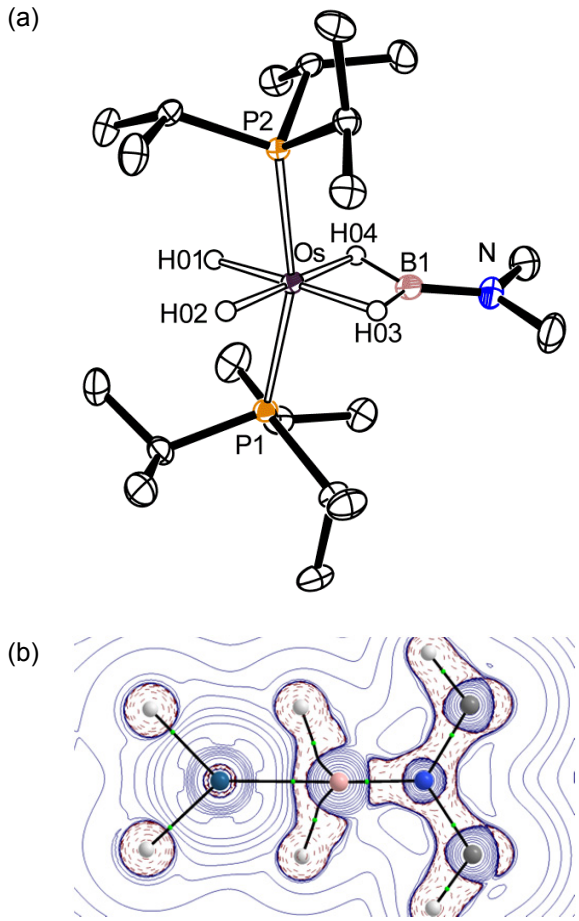


**Figure 7**. (a) Molecular diagram of complex **7** with 50% probability ellipsoids. The hydrogen atoms (except hydrides) are omitted for clarity. Selected bond lengths (Å) and angles (deg) for the X-ray and optimized (in square brackets) structures: Os–H(01) = 1.67(3) [1.659], Os–H(02) = 1.61(3) [1.647], Os–H(03) = 1.64(3) [1.807], Os–H(04) = 1.62(3) [1.839], Os–B = 1.943(3) [1.969], Os–P(1) = 2.3109(6) [2.318], Os–P(2) = 2.3181(6) [2.325], B–H(03) = 1.29(3) [1.382], B–H(04) = 1.31(3) [1.362], B–N = 1.379(4) [1.407]; P(1)–Os–P(2) = 163.20(2) [160.35], H(01)–Os–H(02) = 88.1(13) [88.28], H(01)–Os–H(03) = 174.1(12) [178.59], H(01)–Os–H(04) = 92.7(13) [95.07], H(02)–Os–H(03) = 96.2(13) [92.46], H(02)–Os–H(04) = 179.1(13) [176.60],

H(03)–Os–H(04) = 83.1(13) [84.18], H(03)–B–H(04) = 112.3(17) [125.88], H(03)–B–N = 122.8(4) [116.23], H(04)–B–N = 124.8(12) [117.63]. (b) Contour line diagram $\nabla^2\rho(r)$ for complex **7** in the Os–H–B plane. The solid lines connecting the atomic nuclei are the bond paths while the small green and red spheres indicate the corresponding BCPs and RCPs ring critical points, respectively.

The $^1$H, $^{31}$P{$^1$H}, and $^{11}$B{$^1$H} NMR spectra of **7** and **8**, in toluene-$d_8$, at room temperature are consistent with the structure shown in Figure **9a**. The $^1$H NMR spectra in the high field region show a broad resonance centered at about –9.8 ppm due to the boron bridging atoms and a triplet ($^2J_{H–P} \approx 23$ Hz) close to –10.6 ppm corresponding to the hydride ligands. The $^{31}$P{$^1$H} spectra display a singlet at about 57 ppm for the equivalent phosphines, whereas the $^{11}$B{$^1$H} NMR spectra contain a broad signal centered at 67 ppm for **7** and at 64 ppm for **8**.

## CONCLUDING REMARKS

This study has revealed that $H_2BR_x$ (x = 2, 1) ligands can be coordinated to an unsaturated metal fragment in three different modes, namely $\kappa^2$-*H*,*H*-($H_2BR_2$), $\eta^3$-$H_2BR_2$, and $\eta^2$:$\eta^2$-$H_2BR$. $\kappa^2$-*H*,*H*-($H_2BR_2$) Ligands are formally 3e donor dihydrideborate groups, which form two 3c, 2e M–H–B bonds, similar to the B–H–B bonds of diborane ($B_2H_6$). 3e Donor dihydrideborate groups can also form two bonds with the metal center that resemble the coordination of two elongated $\sigma$-boranes ($\eta^2$-$HBR_2$). As a consequence, in contrast to the $\kappa^2$-*H*,*H*-($H_2BR_2$)-coordination mode, the boron atom interacts significantly with the metal center, generating a $\eta^3$-$H_2BR_2$-coordination, where the B–H bond lengths depend upon the *trans* influence of the coligand *trans* coordinated. The $\eta^3$-$H_2BR_2$-coordination mode should be viewed as an electron deficient situation derived from a $\eta^2$:$\eta^2$-$H_2BR$-coordination of a 4e donor primary borane, where one of the two electrons of the boron atom involved in the $BH_2$ unit has been used to form an additional B–R bond.

In conclusion, herein, we show strong structural and AIM evidence for a new coordination mode of the dihydrideborate groups, which is governed by the coligands coordinated *trans*.

## EXPERIMENTAL SECTION

All manipulations were performed under argon using standard Schlenk-tube or glovebox techniques and dried solvents. Pinacolborane (HBpin = 4,4,5,5-tetramethyl-1,3,2-dioxaborolane) and 9-borabicyclo[3.3.1]nonane dimmer ($(HBbn)_2$) were purchased from commercial sources and used without further purification. Catecholborane (HBcat = 1,3,2-benzodioxaborolane) was purchased from commercial sources and distilled in a Kugelrohr distillation oven. Complex $OsH_6(P^iPr_3)_2$ (**1**) was prepared according to the published method.[32] Instrumental methods used for characterization, X-ray information, and computational details are given in the Supporting Information. Chemical shifts (in ppm) are referenced to residual solvent peaks ($^1H$, $^{13}C\{^1H\}$), external $H_3PO_4$ ($^{31}P\{^1H\}$), or $BF_3{\cdot}OEt_2$ ($^{11}B$). Coupling constants, *J*, and *N* ($N = {}^3J_{H\text{-}P} + {}^5J_{H\text{-}P'}$ for $^1H$ or ${}^1J_{C\text{-}P} + {}^3J_{C\text{-}P'}$ for $^{13}C$) are given in Hertz.

**Preparation of $OsH_3\{\kappa^2\text{-}H,H\text{-}(H_2Bbn)(P^iPr_3)_2$ (2).** 9-Borabicyclo(3.3.1)nonane (22 mg, 0.090 mmol) was added to a solution of **1** (100 mg, 0.193 mmol) in 5 mL of toluene and it was heated at 110 ºC for 18 h. After cooling at room temperature, the solvent was removed under reduced pressure to afford a yellow solid that was washed with pentane (2 x 1 mL) and dried in vacuo. Yield: 63.8 mg (50%). Yellow crystals suitable for X-ray diffraction analysis were grown from a solution of **2** in pentane at –30 ºC. Anal. Calcd for $C_{26}H_{61}BOsP_2$: C, 49.04; H, 9.66. Found: C, 49.39; H, 9.40. IR ($cm^{-1}$): ν(Os–H) 2124 (m). $^1H$ NMR (300.13 MHz, $C_6D_6$, 298 K): δ 2.14 (m, 6H, Bbn), 1.98 (m, 4H, Bbn), 1.85 (m, 6H, CH $^i$Pr), 1.77 (m, 4H, Bbn), 1.12 (dvt, ${}^3J_{H\text{-}H} = 6.0$, $N =$ 14.0, 36H, $CH_3$ $^i$Pr), −10.43 (br, 5H, $OsH_5$). $^1H$ NMR (400.13 MHz, $C_7D_8$, 183 K): δ 2.22 (br, 6H, CH $^i$Pr), 1.91 (br, 4H, $CH_2$ BBN), 1.75 (br, 2H, CH Bbn), 1.66 (br, 8H, $CH_2$ Bbn), 1.06 (br,

36H, $CH_3$ $^i$Pr), −7.09 (br, 2H, $OsH_2B$), −12.59 (br, 3H, $OsH_3$). $^{11}B\{^1H\}$ NMR (96.29 MHz, $C_6D_6$, 298 K): δ 44 (br).

**Preparation of $OsH_3\{\kappa^2$-*H*,*H*-$(H_2Bpin)(P^iPr_3)_2$ (3).** Pinacolborane (60 μL, 0.386 mmol) was added to a solution of **1** (100 mg, 0.193 mmol) in 5 mL of toluene and it was heated at 50 ºC for 18 h. After cooling at room temperature, the solvent was removed under reduced pressure to afford an orange oil. The addition of pentane (1 mL) afforded a white solid that was washed with pentane (2 x 1 mL) and dried in vacuo. Yield: 42 mg (33%). Colorless single crystals suitable for X-ray diffraction analysis were grown from a solution of **3** in pentane at –30 ºC. Anal. Calcd for $C_{24}H_{59}BO_2OsP_2$: C, 44.85; H, 9.25. Found: C, 44.71; H, 9.07. IR ($cm^{-1}$): ν(Os–H) 2084 (w), ν(B–H) 1841 (m). $^1H$ NMR (300.13 MHz, $C_6D_6$, 298 K): δ 2.09 (m, 6H, CH $^i$Pr), 1.22 (dvt, $^3J_{H\text{-}H}$ = 6.3, *N* = 13.8, 36H, $CH_3$ $^i$Pr$_3$), 1.13 (s, 12H, Bpin) δ –10.30 (br, 5H, $OsH_5$). $^{31}P\{^1H\}$ NMR (121.4 MHz, $C_7D_8$, 298 K): δ 44.7 (s). $^{11}B\{^1H\}$ NMR (96.29 MHz, $C_6D_6$, 298 K): δ 35 (br).

**Reaction of 1 with catecholborane: Formation of $OsH_3\{\kappa^2$-*H*,*H*-$(H_2Bcat)(P^iPr_3)_2$ (5).** Catecholborane (5.3 μL, 0.05 mmol) was added to a NMR tube containing a solution of **1** (25 mg, 0.05 mmol) in 0.5 mL of toluene-$d_8$. The tube was heated at 50ºC for 18 h. After this time, the NMR spectra showed the presence of **1**, **5** and **6** in a 15:77:8 molar ratio. All attempts to isolate pure **5** were unsuccessful. Data for **5**: $^1H$ NMR (300.13 MHz, $C_7D_8$, 298 K): δ 6.93 (m, 2H, Bcat), 6.72 (m, 2H, Bcat), 2.13 (m, 6H, CH $^i$Pr), 1.15 (dvt, $^3J_{H\text{-}H}$ = 7.0, *N* = 13.6, 36H, $CH_3$ $^i$Pr), –9.61 (br, 5H, $OsH_5$). $^{31}P\{^1H\}$ NMR (121.4 MHz, $C_7D_8$, 298 K): δ 48.0 (s). $^{11}B\{^1H\}$ NMR (96.29 MHz, $C_7D_8$, 298 K): δ 40 (br).

**Preparation of $OsH(\eta^3$-$H_2Bcat)(\eta^2$-$HBcat)(P^iPr_3)_2$ (6)**. Catecholborane (16.0 μL, 0.15 mmol) was added to a NMR tube containing a solution of **1** (25 mg, 0.05 mmol) in 0.5 mL of toluene-$d_8$. The tube was heated at 50 ºC for 18 h. After cooling at room temperature, the solvent was

removed under reduced pressure giving an orange oil. The orange oil was dissolved in pentane and cooled at –30 ºC. After 24 h, colorless single crystals suitable for X-ray diffraction analysis were obtained. Yield: 37.6 mg (27%). Anal. Calcd for $C_{30}H_{54}B_2O_4OsP_2$: C, 47.88 H, 7.23. Found: C, 48.17; H, 7.27. IR ($cm^{-1}$): ν(Os–H) 2072 (w), ν(B–H) 1903 (m, br). $^1$H NMR (300.13 MHz, $C_7D_8$, 298 K): δ 6.91 (m, 4H, Bcat), 6.73 (m, 4H, Bcat), 2.34 (m, 6H, CH $^i$Pr), 1.15 (dvt, $^3J_{H\text{-}H}$ = 6.5, *N* = 13.6, 36H, $CH_3$ $^i$Pr), –9.50 (br, 4H, $OsH_4$). $^{31}$P{$^1$H} NMR (121.4 MHz, $C_7D_8$, 298 K): δ 36.9 (s). $^{11}$B{$^1$H} NMR (96.29 MHz, $C_7D_8$, 298 K): δ 35 (br).

**Preparation of [$OsH_2(\eta^2\text{:}\eta^2\text{-}H_2BNMe_2)(P^iPr_3)_2$] (7).** Dimethylamine–borane (36 mg, 0.60 mmol) was added to a solution of **1** (100 mg, 0.193 mmol) in 5 mL of toluene and it was heated at 80 ºC for 18 h. After cooling at room temperature, the solvent was removed under reduced pressure to afford to afford an orange oil. The addition of pentane (1 mL) afforded a white solid that was washed with pentane (2 x 1 mL) and dried in vacuo. Yield: 42 mg (67%). Colorless single crystals suitable for X-ray diffraction analysis were grown from a solution of **7** in pentane at –78 ºC. Anal. Calcd for $C_{20}H_{52}BNOsP_2$: C, 42.17; H, 9.20; N, 2.46. Found: C, 42.31; H, 9.46; N, 2.32. IR ($cm^{-1}$): ν(Os–H) 2009, 1977 (m), ν(B–H) 1795 (m, br). $^1$H NMR (300.13 MHz, $C_6D_6$, 298 K): δ 2.57 (s, 6H, $NCH_3$), 2.01 (m, 6H, CH $^i$Pr), 1.34 (dvt, $^3J_{H\text{-}H}$ = 6.0, *N* = 12.9, 36H, $CH_3$ $^i$Pr), –9.94 (br, 2H, $OsH_2B$), –10.71 (t, $^2J_{H\text{-}P}$ = 22.8, 2H, $OsH_2$). $^{31}$P{$^1$H} NMR (121.4 MHz, $C_6D_6$, 298 K): δ 57.2 (s). $^{11}$B{$^1$H} NMR (96.29 MHz, $C_6D_6$, 298 K): δ 67 (br).

**Preparation of [$OsH_2(\eta^2\text{:}\eta^2\text{-}H_2BNH^tBu)(P^iPr_3)_2$] (8).** *tert*-Butylamine–borane (52.2 mg, 0.60 mmol) was added to a solution of **1** (100 mg, 0.20 mmol) in 5 mL of toluene and it was heated at 80 ºC for 18 h. After cooling at room temperature, the solvent was removed under reduced pressure to afford to afford an orange oil. Colorless crystals were grown from a solution of **8** in pentane at –78 ºC. Yield: 24 mg (20 %). Anal. Calcd for $C_{22}H_{56}BNOsP_2$: C, 44.21; H, 9.44; N,

2.34. Found: C, 44.41; H, 9.44; N, 2.56. IR ($cm^{-1}$): ν(N–H) 3398 (w), ν(Os–H) 1985 (w), ν(B–H) 1801, 1811 (m, br). $^{1}H$ NMR (300.13 MHz, $C_6D_6$, 298 K): δ 2.08 (m, 6H, CH $^{i}Pr$), 1.93 (br, 1H, NH), 1.39 (dvt, $^{3}J_{H-H}$ = 7.0, *N* = 12.9, 36H, $CH_3$ $^{i}Pr$), 1.17 (s, 9H, $CH_3$ $^{t}Bu$), –9.78(br, 2H, $OsH_2B$), –10.59 (t, $^{2}J_{H-P}$ = 23.3, 2H, $OsH_2$). $^{31}P\{^{1}H\}$ NMR (121.4 MHz, $C_6D_6$, 298 K): δ 56.8 (s). $^{11}B\{^{1}H\}$ NMR (96.29 MHz, $C_6D_6$, 298 K): δ 64 (br).

ASSOCIATED CONTENT

**Supporting Information**. The following files are available free of charge.

General information, crystallographic data, computational details, NMR and IR spectra of complexes **2**, **3**, **5**, **6**, **7**, and **8**, and total energies of **2–7** (PDF)

Cartesian coordinates of **2–7** (XYZ)

**Accession Codes**

CCDC 1815982–1815985 contain the supplementary crystallographic data for this paper. These data can be obtained free of charge via www.ccdc.cam.ac.uk/data_request/cif, or by emailing data_ request@ccdc.cam.ac.uk, or by contacting The Cambridge Crystallographic Data Centre, 12 Union Road, Cambridge CB2 1EZ, UK; fax: +44 1223 336033.

**AUTHOR INFORMATION**

**Corresponding Author**

*E-mail: master@unizar.es.

**Author Contributions**

The manuscript was written through contributions of all authors. All authors have given approval to the final version of the manuscript.

**ACKNOWLEDGMENT**

Financial support from the Spanish MINECO (Projects CTQ2017-82935-P, CTQ2016-78205-P, Red de Excelencia Consolider CTQ2016-81797-REDC), Gobierno de Aragón (E35), FEDER, and the European Social Fund (FSE) is acknowledged.

REFERENCES

(1) Esteruelas, M. A.; López, A. M.; Oliván, M. Polyhydrides of Platinum Group Metals: Nonclassical Interactions and σ‑Bond Activation Reactions. *Chem. Rev*. **2016**, *116*, 8770–8847.

(2) Kubas, G. J. Metal Dihydrogen and σ-Bond Complexes: Structure, Theory and Reactivity; Kluwer: New York, 2001. (b) Kubas, G. J. Metal–dihydrogen and σ‑bond coordination: the consummate extension of the Dewar–Chatt–Duncanson model for metal–olefin π bonding. *J. Organomet. Chem*. **2001**, *635*, 37–68. (c) Kubas, G. J. Heterolytic Splitting of H−H, Si−H, and Other Bonds on Electrophilic Metal Centers. *Adv. Inorg. Chem*. **2004**, *56*, 127–177. (d) Kubas, G. J. Fundamentals of $H_2$ Binding and Reactivity on Transition Metals Underlying Hydrogenase Function and $H_2$ Production and Storage. *Chem. Rev*. **2007**, *107*, 4152–4205. (e) Kubas, G. J. Activation of dihydrogen and coordination of molecular $H_2$ on transition metals. *J. Organomet. Chem*. **2014**, *751*, 33–49. (f) Crabtree, R. H. Dihydrogen Complexation. *Chem. Rev*. **2016**, *116*, 8750–8769.

(3) Perutz, R. N.; Sabo-Etienne, S. The σ-CAM Mechanism: σ Complexes as the Basis of σ-Bond Metathesis at Late-Transition-Metal Centers. *Angew. Chem., Int. Ed*. **2007**, *46*, 2578–2592. (b) Alcaraz, G.; Grellier, M.; Sabo-Etienne, S. Bis σ-Bond Dihydrogen and Borane Ruthenium Complexes: Bonding Nature, Catalytic Applications, and Reversible Hydrogen Release. *Acc. Chem. Res*. **2009**, *42*, 1640–1649. (c) Pandey, K. K. Transition metal–borane complexes. *Coord. Chem. Rev*. **2009**, *253*, 37–55. (d) Braunschweig, H.; Dewhurst, R. D.; Schneider, A. Electron-Precise Coordination Modes of Boron-Centered Ligands. *Chem. Rev*. **2010**, *110*, 3924–3957.

(4) Miyaura, N. Metal-Catalyzed Reactions of Organoboronic Acids and Esters. *Bull. Chem. Soc. Jpn*. **2008**, *81*, 1535–1553. (b) Crudden, C. M.; Glasspoole, B. W.; Lata, C. J. Expanding the scope of transformations of organoboron species: carbon–carbon bond formation with retention of configuration. *Chem. Commun*. **2009**, 6704–6716. (c) Dang, L.; Lin, Z. Y.; Marder, T. B. Boryl ligands and their roles in metal-catalysed borylation reactions. *Chem. Commun*. **2009**, 3987–3995. (d) Mkhalid, I. A. I.; Barnard, J. H.; Marder, T. B.; Murphy, J. M.; Hartwig, J. F. C–H Activation for the Construction of C–B Bonds. *Chem. Rev*. **2010**, *110*, 890–931. (e) Ros, A.; Fernández, R.; Lassaletta, J. M. Functional group directed C–H borylation. *Chem. Soc. Rev*. **2014**, *43*, 3229–3243. (f) Xu, L.; Wang, G.; Zhang, S.; Wang, H.; Wang, L.; Liu, L.; Jiao, J.; Li, P. Recent advances in catalytic C–H borylation reactions. *Tetrahedron* **2017**, *7*3, 7123–7157.

(5) Hamilton, C. W.; Baker, R. T.; Staubitz, A.; Manners, I. B–N compounds for chemical hydrogen storage. *Chem. Soc. Rev*. **2009**, *38*, 279–293. (b) Waterman, R. Mechanisms of metal-catalyzed dehydrocoupling reactions. *Chem. Soc. Rev*. **2013**, *42*, 5629–5641. (c) St. John, A.; Goldberg, K. I.; Heinekey, D. M. Pincer Complexes as Catalysts for Amine Borane Dehydrogenation. *Top. Organomet. Chem*. **2013**, *40*, 271–287. (d) Rossin, A.; Peruzzini, M. Ammonia−Borane and Amine−Borane Dehydrogenation Mediated by Complex Metal Hydrides.

*Chem. Rev*. **2016**, *116*, 8848–8872. (e) Bhunya, S.; Malakar, T.; Ganguly, G.; Paul, A. Combining Protons and Hydrides by Homogeneous Catalysis for Controlling the Release of Hydrogen from Ammonia–Borane: Present Status and Challenges. *ACS Catal*. **2016**, *6*, 7907–7934.

(6) Bader, R. F. W. *Atoms in Molecules. A Quantum Theory*; Oxford University Press: Oxford, U.K., 1990.

(7) Hesp, K. D.; Kannemann, F. O.; Rankin, M. A.; McDonald, R.; Ferguson, M. J.; Stradiotto, M. Probing Mesitylborane and Mesitylborate Ligation Within the Coordination Sphere of Cp*Ru($P^iPr_3$)$^+$: A Combined Synthetic, X-ray Crystallographic, and Computational Study. *Inorg. Chem.* **2011**, *50*, 2431–2444. (b) Bénac-Lestrille, G.; Helmstedt, U.; Vendier, L.; Alcaraz, G.; Clot, E.; Sabo-Etienne, S. Dimethylaminoborane ($H_2BNMe_2$) Coordination to Late Transition Metal Centers: Snapshots of the B–H Oxidative Addition Process. *Inorg. Chem.* **2011**, *50*, 11039–11045. (c) Buil, M. L.; Cardo, J. J. F.; Esteruelas, M. A.; Fernández, I.; Oñate, E. Hydroboration and Hydrogenation of an Osmium–Carbon Triple Bond: Osmium Chemistry of a Bis-*σ*-Borane. *Organometallics* **2015**, *34*, 547–550.

(8) Kumar, A.; Beattie, N. A.; Pike, S. D.; Macgregor, S. A.; Weller, A. S. The Simplest Amino-borane $H_2B{=}NH_2$ Trapped on a Rhodium Dimer: Pre-Catalysts for Amine–Borane Dehydropolymerization. *Angew. Chem., Int. Ed.* **2016**, *55*, 6651–6656.

(9) Esteruelas, M. A.; Fernández-Álvarez, F. J.; López, A. M.; Mora, M.; Oñate, E. Borinium Cations as *σ*-B-H Ligands in Osmium Complexes *J. Am. Chem. Soc.* **2010**, *132*, 5600–5601. (b) Buil, M. L.; Cardo, J. J. F.; Esteruelas, M. A.; Fernández, I.; Oñate, E. Unprecedented Addition of Tetrahydroborate to an Osmium–Carbon Triple Bond. *Organometallics* **2014**, *33*, 2689–2692.

(c) Pandey, K. K. What is the best bonding model of the (σ-H-BR) species bound to a transition metal? Bonding analysis in complexes [$(H)_2Cl(PMe_3)_2M$(σ-H-BR)] (M = Fe, Ru, Os). *Dalton Trans*., **2012**, *41*, 3278–3286.

(10) Esteruelas, M. A.; Fenández, I.; García-Yebra, C.; Martín, J.; Oñate, E. Elongated σ-Borane versus σ-Borane in Pincer–POP–Osmium Complexes *Organometallics* **2017**, *36*, 2298–2307.

(11) Miyada, T.; Kwan, E. H.; Yamashita, M. Synthesis, Structure, and Bonding Properties of Ruthenium Complexes Possessing a Boron-Based PBP Pincer Ligand and Their Application for Catalytic Hydrogenation. *Organometallics* **2014**, *33*, 6760–6770. (b) Drover, M. W.; Bowes, E. G.; Schafer, L. L.; Love, J. A.; Weller, A. S. Phosphoramidate-Supported $Cp^*Ir^{III}$ Aminoborane $H_2B{=}NR_2$ Complexes: Synthesis, Structure, and Solution Dynamics. *Chem. - Eur. J.* **2016**, *22*, 6793–6797.

(12) A bond critical point (BCP) is the point of minimum electron density along a bond path. When the bond paths are disposed to form a ring of bonded atoms an additional critical point (ring critical point, RCP) is found in the inner of the ring.

(13) (a) Hebden, T. J.; Denney, M. C.; Pons, V.; Piccoli, P. M. B.; Koetzle, T. F.; Schultz, A. J.; Kaminsky, W.; Goldberg, K. I.; Heinekey, D. M. *σ*-Borane Complexes of Iridium: Synthesis and Structural Characterization. *J. Am. Chem. Soc.* **2008**, *130*, 10812–10820. (b) Esteruelas, M. A.; López, A. M.; Mora, M.; Oñate, E. B–H activation and H–H formation: two consecutive heterolytic processes on an osmium–hydrogensulfide bond. *Chem. Commun.* **2013**, *49*, 7543–7545.

(14) (a) Alcaraz, G.; Clot, E.; Helmstedt, U.; Vendier, L.; Sabo-Etienne, S. Mesitylborane as a Bis(σ-B–H) Ligand: An Unprecedented Bonding Mode to a Metal Center. *J. Am. Chem. Soc.* **2007**, *129*, 8704–8705. (b) Gloaguen, Y.; Alcaraz, G.; Vendier, L.; Sabo-Etienne, S. *Tert*-butylborane: A bis (σ-B–H) ligand in ruthenium hydride chemistry. *J. Organomet. Chem.* **2009**, *694*, 2839–2841. (c) Douglas, T. M.; Chaplin, A. B.; Weller, A. S.; Yang, X.; Hall, M. B. Monomeric and Oligomeric Amine-Borane σ-Complexes of Rhodium. Intermediates in the Catalytic Dehydrogenation of Amine-Boranes. *J. Am. Chem. Soc.* **2009**, *131*, 15440–15456. (d) Alcaraz, G.; Vendier, L.; Clot, E.; Sabo-Etienne, S. Ruthenium Bis(σ-B–H) Aminoborane Complexes from Dehydrogenation of Amine–Boranes: Trapping of $H_2B$–$NH_2$. *Angew. Chem., Int. Ed*. **2010**, *49*, 918–920. (e) Alcaraz, G.; Chaplin, A. B.; Stevens, C. J.; Clot, E.; Vendier, L.; Weller, A. S.; Sabo-Etienne, S. Ruthenium, Rhodium, and Iridium Bis(σ-B-H) Diisopropylaminoborane Complexes. *Organometallics* **2010**, 29, 5591–5595. (f) Tang, C. Y.; Thompson, A. L.; Aldridge, S. Dehydrogenation of Saturated CC and BN Bonds at Cationic N-Heterocyclic Carbene Stabilized M(III) Centers (M = Rh, Ir). *J. Am. Chem. Soc.* **2010**, *132*, 10578–10591. (g) Stevens, C. J.; Dallanegra, R.; Chaplin, A. B.; Weller, A. S.; Macgregor, S. A.; Ward, B.; McKay, D.; Alcaraz, G.; Sabo-Etienne, S. $[Ir(PCy_3)_2(H)_2(H_2B\text{-}NMe_2)]^+$ as a Latent Source of Aminoborane: Probing the Role of Metal in the Dehydrocoupling of $H_3B{\cdot}NMe_2H$ and Retrodimerisation of $[H_2BNMe_2]_2$. *Chem. - Eur. J.* **2011**, *17*, 3011–3020. (h) Tang, C. Y.; Phillips, N.; Bates, J. I.; Thompson, A. L.; Gutmann, M. J.; Aldridge, S. Dimethylamine borane dehydrogenation chemistry: syntheses, X-ray and neutron diffraction studies of 18-electron aminoborane and 14-electron aminoboryl complexes. *Chem. Commun.* **2012**, *48*, 8096–8098. (i) Gloaguen, Y.; Benac-Lestrille, G.; Vendier, L.; Helmstedt, U.; Clot, E.; Alcaraz, G.; Sabo-Etienne, S. Monosubstituted Borane Ruthenium Complexes $RuH_2(\eta^2{:}\eta^2\text{-}H_2BR)(PR'_3)_2$: A

General Approach to the Geminal Bis(σ-B–H) Coordination Mode. *Organometallics* **2013**, *32*, 4868–4877. (j) Phillips, N.; Tang, C. Y.; Tirfoin, R.; Kelly, M. J.; Thompson, A. L.; Gutmann, M. J.; Aldridge, S. Modulating reactivity in iridium bis(N-heterocyclic carbene) complexes: influence of ring size on E–H bond activation chemistry. *Dalton Trans.* **2014**, *43*, 12288–12298.

(15) (a) Antiñolo, A.; Carrillo-Hermosilla, F.; Fernández-Baeza, J.; García-Yuste, S.; Otero, A.; Rodríguez, A. M.; Sánchez-Prada, J.; Villasenor, E.; Gelabert, R.; Moreno, M.; Lluch, J. M.; Lledós, A. Structure and Dynamics of [Nb($\eta^5$-$C_5H_4SiMe_3$)$_2$($\eta^2$-$H_2BR_2$)] ($R_2$ = $O_2C_6H_4$, $C_8H_{14}$, $H_2$) Complexes. A Combined Experimental and Theoretical Study. *Organometallics* **2000**, *19*, 3654–3663. (b) Montiel-Palma, V.; Lumbierres, M.; Donnadieu, B.; Sabo-Etienne, S.; Chaudret, B. σ-Borane and Dihydroborate Complexes of Ruthenium. *J. Am. Chem. Soc.* **2002**, *124*, 5624–5625. (c) Westcott, S. A.; Marder, T. B.; Baker, R. T.; Harlow, R. L.; Calabrese, J. C.; Lam, K. C.; Lin, Z. Reactions of hydroborating reagents with phosphinorhodium hydride complexes: molecular structures of a $Rh_2B_3$ metallaborane cluster, an $L_2Rh(\eta^2$-$H_2BR_2)$ complex and a mixed valence Rh dimer containing a semi-bridging Bcat (cat = 1,2-$O_2C_6H_4$) group. Polyhedron **2004**, *23*, 2665–2677. (d) Lachaize, S.; Essalah, W.; Montiel-Palma, V.; Vendier, L.; Chaudret, B.; Barthelat, J.-C.; Sabo-Etienne, S. Coordination Modes of Boranes in Polyhydride Ruthenium Complexes: σ-Borane versus Dihydridoborate. *Organometallics* **2005**, *24*, 2935–2943. (e) Bontemps, S.; Vendier, L.; Sabo-Etienne, S. Borane-Mediated Carbon Dioxide Reduction at Ruthenium: Formation of $C_1$ and $C_2$ Compounds. *Angew. Chem., Int. Ed.* **2012**, *51*, 1671–1674. (f) Gunanathan, C.; Hölscher, M.; Pan, F. F.; Leitner, W. Ruthenium Catalyzed Hydroboration of Terminal Alkynes to *Z*−Vinylboronates *J. Am. Chem. Soc.* **2012**, *134*, 14349–14352. (g) Chakraborty, S.; Zhang, J.; Patel, Y. J.; Krause, J. A.; Guan, H. Pincer-Ligated Nickel Hydridoborate Complexes: the Dormant Species in Catalytic Reduction of Carbon

Dioxide with Boranes. *Inorg. Chem.* **2013**, *52*, 37−47. (h) Esteruelas, M. A.; López, A. M.; Mora, M.; Oñate, E. Boryl-Dihydrideborate Osmium Complexes: Preparation, Structure, and Dynamic Behavior in Solution. *Organometallics* **2015**, *34*, 941−946. (i) Arnold, N.; Mozo, S.; Paul, U.; Radius, U.; Braunschweig, H. Aryldihydroborane Coordination to Iridium and Osmium Hydrido Complexes. *Organometallics* **2015**, *34*, 5709−5715. (j) Kumar, A.; Ishibashi, J. S. A.; Hooper, T. N.; Mikulas, T. C.; Dixon, D. A.; Liu, S. Y.; Weller, A. S. The Synthesis, Characterization and Dehydrogenation of Sigma-Complexes of BN-Cyclohexanes. *Chem. - Eur. J.* **2016**, *22*, 310−322.

(16) Brugos, J.; Cabeza, J. A.; García-Álvarez, P.; Kennedy, A. R.; Pérez-Carreño, E.; Van der Maelen, J. F. 2-(Methylamido)pyridine−Borane: A Tripod $\kappa^3$-N,H,H Ligand in Trigonal Bipyramidal Rhodium(I) and Iridium(I) Complexes with an Asymmetric Coordination of Its $BH_3$ Group. *Inorg. Chem.* **2016**, *55*, 8905−8912.

(17) Buil, M. L.; Cardo, J. J. F.; Esteruelas, M. A.; Fernández, I.; Oñate, E. An Entry to Stable Mixed Phosphine−Osmium−NHC Polyhydrides. *Inorg. Chem.* **2016**, *55*, 5062−5070.

(18) (a) Buil, M. L.; Esteruelas, M. A.; Garcés, K.; Oñate, E. From Tetrahydroborate- to Aminoborylvinylidene-Osmium Complexes via Alkynyl-Aminoboryl Intermediates. *J. Am. Chem. Soc.* **2011**, *133*, 2250−2263. (b) Esteruelas, M. A.; Fernández, I.; López, A. M.; Mora, M.; Oñate, E. Preparation, Structure, Bonding, and Preliminary Reactivity of a Six-Coordinate $d^4$ Osmium−Boryl Complex. *Organometallics* **2012**, *31*, 4646−4649. (c) Esteruelas, M. A.; Fernández, I.; López, A. M.; Mora, M.; Oñate, E. Osmium-Promoted Dehydrogenation of Amine−Boranes and B−H Bond Activation of the Resulting Amino−Boranes. *Organometallics* **2014**, *33*, 1104−1107. (d) Esteruelas, M. A.; López, A. M.; Mora, M.; Oñate, E. Ammonia-

Borane Dehydrogenation Promoted by an Osmium Dihydride Complex: Kinetics and Mechanism. *ACS Catal.* **2015**, *5*, 187−191.

(19) (a) Esteruelas, M. A.; Masamunt, A. B.; Oliván, M.; Oñate, E.; Valencia, M. Aromatic Diosmatricyclic Nitrogen-Containing Compounds. *J. Am. Chem. Soc.* **2008**, *130*, 11612−11613. (b) Crespo, O.; Eguillor, B.; Esteruelas, M. A.; Fernández, I.; García-Raboso, J.; Gómez-Gallego, M.; Martín-Ortiz, M.; Oliván, M.; Sierra, M. A. Synthesis and characterisation of [6]-azaosmahelicenes: the first $d^4$-heterometallahelicenes. *Chem. Commun.* **2012**, *48*, 5328−5330. (c) Alabau, R. G.; Eguillor, B.; Esler, J.; Esteruelas, M. A.; Oliván, M.; Oñate, E.; Tsai, J.-Y.; Xia, C. J. CCC−Pincer−NHC Osmium Complexes: New Types of Blue-Green Emissive Neutral Compounds for Organic Light-Emitting Devices (OLEDs). *Organometallics* **2014**, *33*, 5582−5596. (d) Bolaño, T.; Esteruelas, M. A.; Fernández, I.; Oñate, E.; Palacios, A.; Tsai, J.-Y.; Xia, C. J. Osmium(II)−Bis(dihydrogen) Complexes Containing $C_{aryl}$,$C_{NHC}$−Chelate Ligands: Preparation, Bonding Situation, and Acidity. *Organometallics* **2015**, *34*, 778−789. (e) Esteruelas, M. A.; Larramona, C.; Oñate, E. Osmium-Mediated Direct C−H Bond Activation at the 8-Position of Quinolines. *Organometallics* **2016**, *35*, 1597−1600. (f) Eguillor, B.; Esteruelas, M. A.; Lezáun, V.; Oliván, M.; Oñate, E.; Tsai, J.-Y.; Xia, C. J. A Capped Octahedral $MHC_6$ Compound of a Platinum Group Metal. *Chem. - Eur. J.* **2016**, *22*, 9106−9110. (g) Alabau, R. G.; Esteruelas, M. A.; Oliván, M.; Oñate, E.; Palacios, A. U.; Tsai, J.-Y.; Xia, C. J. Osmium(II) Complexes Containing a Dianionic CCCC-Donor Tetradentate Ligand. *Organometallics* **2016**, *35*, 3981−3995. (h) Eguillor, B.; Esteruelas, M. A.; Lezáun, V.; Oliván, M.; Oñate, E. Elongated Dihydrogen versus Compressed Dihydride in Osmium Complexes. *Chem. - Eur. J.* **2017**, *23*, 1526−1530.

(20) (a) Esteruelas, M. A.; García-Raboso, J.; Oliván, M.; Oñate, E. N–H and N–C Bond Activation of Pyrimidinic Nucleobases and Nucleosides Promoted by an Osmium Polyhydride. *Inorg. Chem.* **2012**, *51*, 5975–5984. (b) Esteruelas, M. A.; García-Raboso, J.; Oliván, M. Reactions of an Osmium-Hexahydride Complex with Cytosine, Deoxycytidine, and Cytidine: The Importance of the Minor Tautomers. *Inorg. Chem.* **2012**, *51*, 9522–9528. (c) Casarrubios, L.; Esteruelas, M. A.; Larramona, C.; Muntaner, J. G.; Oliván, M.; Oñate, E.; Sierra, M. A. Chelated Assisted Metal-Mediated N–H Bond Activation of β-Lactams: Preparation of Irida-, Rhoda-, Osma-, and Ruthenatrinems. *Organometallics* **2014**, *33*, 1820–1833. (d) Alabau, R. G.; Esteruelas, M. A.; Oliván, M.; Oñate, E. Preparation of Phosphorescent Osmium(IV) Complexes with N,N',C and C,N,C'-Pincer Ligands. *Organometallics* **2017**, *36*, 1848–1859.

(21) (a) Eguillor, B.; Esteruelas, M. A.; García-Raboso, J.; Oliván, M.; Oñate, E.; Pastor, I. M.; Peñafiel, I.; Yus, M. Osmium NHC Complexes from Alcohol-Functionalized Imidazoles and Imidazolium Salts. *Organometallics* **2011**, *30*, 1658–1667. (b) Esteruelas, M. A.; García-Raboso, J.; Oliván, M. Preparation of Half-Sandwich Osmium Complexes by Deprotonation of Aromatic and Pro-aromatic Acids with a Hexahydride Brønsted Base. *Organometallics* **2011**, *30*, 3844–3852.

(22) (a) Casarrubios, L.; Esteruelas, M. A.; Larramona, C.; Lledós, A.; Muntaner, J. G.; Oñate, E.; Ortuño, M. A.; Sierra, M. A. Mechanistic Insight into the Facilitation of β-Lactam Fragmentation through Metal Assistance. *Chem. - Eur. J.* **2015**, *21*, 16781–16785. (b) Casarrubios, L.; Esteruelas, M. A.; Larramona, C.; Muntaner, J. G.; Oñate, E.; Sierra, M. A. 2-Azetidinones as Precursors of Pincer Ligands: Preparation, Structure, and Spectroscopic Properties of CC'N-Osmium Complexes. *Inorg. Chem.* **2015**, *54*, 10998–11006.

(23) Bolaño, T.; Esteruelas, M. A.; Gay, M. P.; Oñate, E.; Pastor, I. M.; Yus, M. An Acyl-NHC Osmium Cooperative System: Coordination of Small Molecules and Heterolytic B–H and O–H Bond Activation. *Organometallics* **2015**, *34*, 3902–3908.

(24) Eguillor, B.; Esteruelas, M. A.; García-Raboso, J.; Oliván, M.; Oñate, E. Stoichiometric and Catalytic Deuteration of Pyridine and Methylpyridines by H/D Exchange with Benzene-$d_6$ Promoted by an Unsaturated Osmium Tetrahydride Species. *Organometallics* **2009**, *28*, 3700–3709.

(25) Werner, H.; Esteruelas, M. A.; Meyer, U.; Wrackmeyer, B. ($\eta^2$-Tetrahydroborato)ruthenium(II)-und-osmium(II)-Komplexe mit fluktuierender Struktur. *Chem. Ber.* **1987**, *120*, 11–15.

(26) Frost, P. W.; Howard, J. A. K.; Spencer, J. L. An Osmium Tetrahydroborate Complex with Unusual Dynamic Behaviour: X-Ray Crystal Structure of $[Os(BH_4)H_3\{P(c\text{-}C_5H_9)_3\}_2]$ (c-$C_5H_9$ = cyclo-$C_5H_9$). *J. Chem. Soc. Chem. Commun.* **1984**, 1362–1363. (b) Esteruelas, M. A.; Jean, Y.; Lledós, A.; Oro, L. A.; Ruiz, N.; Volatron, F. Preparation and Spectroscopic and Theoretical Characterization of the Tetrahydroborate Complex $OsH_3(\eta^2\text{-}H_2BH_2)(P\text{-}i\text{-}Pr_3)_2$. *Inorg. Chem.* **1994**, *33*, 3609–3611. (c) Demachy, I.; Esteruelas, M. A.; Jean, Y.; Lledós, A.; Maseras, F.; Oro, L. A.; Valero, C.; Volatron, F. Hydride Exchange Processes in the Coordination Sphere of Transition Metal Complexes: The $OsH_3(BH4)(PR_3)_2$ System. *J. Am. Chem. Soc.* **1996**, *118*, 8388–8394.

(27) (a) Barrio, P.; Castarlenas, R.; Esteruelas, M. A.; Oñate, E. Triple C–H Activation of a Cycloalkyl Ketone Using an Osmium–Hexahydride Complex. *Organometallics* **2001**, *20*, 2635–2638. (b) Barrio, P.; Esteruelas, M. A.; Oñate, E. Activation of C($sp^2$)-H and Reduction of

C=E (E = CH, N) Bonds with an Osmium-Hexahydride Complex: Influence of E on the Behavior of RCH=E-py Substrates. *Organometallics* **2004**, *23*, 3627−3639. (c) Baya, M.; Eguillor, B.; Esteruelas, M. A.; Lledós, A.; Olivan, M.; Oñate, E. Coordination and Rupture of Methyl C($sp^3$)–H Bonds in Osmium–Polyhydride Complexes with δ Agostic Interaction. *Organometallics* **2007**, *26*, 5140−5152.

(28) (a) Duckett, S. B.; Lowe, J. C.; Lowe, J. P.; Mawby, R. J. Roles of a tetrahydroborate ligand in a facile route to ruthenium(II) ethyl hydride complexes, and a kinetic study of ethane reductive elimination. *Dalton Trans.* **2004**, 3788−3797. (b) Duckett, S. B.; Lowe, J. P.; Mawby, R. J. Use of the tetrahydroborate ligand as "gate-keeper" and protected hydride ligand: preparation and study of alkyl hydride and acyl hydride complexes of ruthenium(II). *Dalton Trans.* **2006**, 2661−2670.

(29) Aldridge, S.; Calder, R. J.; Rossin, A.; Dickinson, A. A.; Willock, D. J.; Jones, C.; Evans, D. J.; Steed, J. W.; Light, M. E.; Coles, S. J.; Hursthouse, M. B. Linking of metal centres through boryl ligands: synthesis, spectroscopic and structural characterisation of symmetrically bridged boryl complexes. *J. Chem. Soc., Dalton Trans*. **2002**, 2020–2026.

(30) Hartwig, J. F.; Cook, K. S.; Hapke, M.; Incarvito, C. D.; Fan, Y.; Webster, C. E.; Hall, M. B. Rhodium Boryl Complexes in the Catalytic, Terminal Functionalization of Alkanes. *J. Am. Chem. Soc.* **2005**, *127*, 2538−2552.

(31) (a) Esteruelas, M. A.; López, A. M.; Mora, M.; Oñate, E. Reactions of Osmium−Pinacolboryl Complexes: Preparation of the First Vinylideneboronate Esters. *Organometallics* **2012**, *31*, 2965−2970. (b) Buil, M. L.; Esteruelas, M. A.; Fernández, I.;

Izquierdo, S.; Oñate, E. Cationic Dihydride Boryl and Dihydride Silyl Osmium(IV) NHC Complexes: A Marked Diagonal Relationship. *Organometallics* **2013**, *32*, 2744−2752.

(32) Aracama, M.; Esteruelas, M. A.; Lahoz, F. J.; López, J. A.; Meyer, U.; Oro, L. A.; Werner, H. Synthesis, Reactivity, Molecular Structure, and Catalytic Activity of the Novel Dichlorodihydridoosmium(IV) Complexes $OsH_2Cl_2(PR_3)_2$ ($PR_3$ = P-*i*-$Pr_3$, PMe-*t*-$Bu_2$). *Inorg.Chem.*, **1991**, *30*, 288−293.

SYNOPSIS: A novel coordination mode of a dihydrideborate ligand to an osmium center featuring two elongated σ-BH bonds has been characterized by X-ray crystallography and by the Atoms in Molecules (AIM) method.

For Table of Contents Only